

End-gas autoignition in premixed hydrogen/air mixture

Hao Yu, Zheng Chen

SKLTCS, Department of Mechanics and Engineering Science, College of Engineering,
Peking University, Beijing 100871, China

1 Introduction

Boosted direct injection spark ignition (DISI) engine is promising since it has higher fuel efficiency and higher power density compared to traditional gasoline engine. However, in highly-boosted gasoline engines operating at low-speed high-load regime, there is strong tendency of knock since the premixture is compressed to high temperature and pressure [1-3]. When knock occurs, high frequency pressure oscillation can cause severe engine damage. It is generally accepted that knock in spark ignition engine (SIE) might be caused by end-gas autoignition [4-6]. When premixed flame propagates in a closed chamber, the unburned gas (end-gas) is progressively compressed by the thermal expansion of burned gas and its temperature and pressure continuously increase. Under appropriate conditions, end-gas autoignition occurs before it is consumed by the propagating flame front. Pressure waves generated by local heat release during autoignition propagate across the system. The unburned mixture immediately behind the pressure wave might be compressed to react rapidly and, in turn, further enhance these waves [3, 4, 6]. A detonation develops if there is a coherent coupling of pressure waves with heat release at the local autoignition kernel [7, 8]. Consequently, high-frequency pressure oscillation or knock occurs.

In the literature, there have been considerable investigations on end-gas autoignition since it is closely related to knock. Livengood and Wu [9] first proposed an integral method to predict the occurrence of autoignition. Zel'dovich [10] first analyzed different modes for propagating reaction fronts caused by autoignition with non-uniform reactivity. Bradley and coworkers [5, 11-13] further investigated the propagation modes of autoignition front caused by a hot spot. They found an operational peninsula, within which detonations can develop at a hot spot.

Experimentally, high speed photograph technology was used to visualize the end-gas autoignition in engine (e.g., [1, 14]) or rapid compression machine (RCM) [3, 15]. In engine or RCM, the flame front and flow are 3D and thereby it is difficult to understand the autoignition process. To overcome this difficulty, Nagano et al. [16] and Qi et al. [17] designed a quasi 1D experiment using a constant volume tube-shaped vessel to study the end-gas autoignition process and pressure oscillation. In these experiments, end-gas autoignition was successfully observed. However, the process is not truly 1D since there is strong flame-boundary layer interaction for flame propagation in a tube. The truly 1D experiment for end-gas autoignition is to use a spherical bomb in which pre-mixture is preheated to high temperature and it autoignites after being compressed by the expanding spherical flame [18]. However, the spherical bomb might be damaged by the strong pressure oscillation or detonation induced by end-gas autoignition.

Multi-dimensional simulations have been conducted to investigate the end-gas autoignition process (e.g., [19-22]). Similar to experiments, the autoignition process is very complicated in multi-dimensional simulations. Moreover, the complicated chemistry involved in ignition is difficult to be included in

multi-dimensional simulation. Therefore, 1-D simulations have been conducted to study the autoignition process. For examples, Ju et al. [23] identified different flame regimes of ignition in n-heptane/air mixtures using 1D simulation with reduced chemistry; and Martz et al. [24] found that the autoignition process is chemically controlled while diffusion can be neglected. However, as mentioned by Reitz and coworkers [25], knocking is still at an early stage of understanding. The detailed mechanism of autoignition induced pressure wave and detonation has not been fully explained in previous studies on end-gas autoignition.

The objectives of this study are to identify possible autoignition modes of end-gas and to investigate the pressure wave and reaction interaction using 1D simulation with detailed chemistry. While multidimensional experiments and simulations mentioned above describe the end-gas autoignition process similar to that occurs in practice, 1D simulations can give more details and insights into the mechanism of autoignition and pressure wave-reaction interaction. Recently, Kagan and Sivashinsky [26, 27] have analyzed the end-gas autoignition in a 1D closed chamber and proposed a 0D model to predict autoignition. However, one-step chemistry was considered in their theoretical analysis. Since complicated chemistry is involved in the ignition process, detailed chemistry needs to be considered for the analysis of autoignition process of real fuels.

2 Numerical models

The emphasis of this study is focused on the mechanism and modes of end-gas autoignition. Therefore, we conduct simulation for stoichiometric H_2 /air mixture since the chemical mechanism for hydrogen oxidation is relatively well established.

One-dimensional flame propagation and autoignition in a closed chamber is simulated using the in-house code A-SURF [28, 29]. A-SURF solves the conservation equations for one-dimensional, compressible, multi-component, reactive flow using the finite volume method. The details on governing equations, numerical scheme and code validation can be found in Refs. [28, 29]. Detailed chemical reaction mechanism of H_2 /air mixture [30] is employed in the simulation. To maintain adequate numerical resolution, dynamically adaptive mesh is utilized so that the reaction zone, pressure wave, shock wave, and detonation are always fully covered by the finest meshes of 0.5 μm . The corresponding time step is 10^{-4} μs since explicit integration method is used. In our previous study [28], it was shown that A-SURF can accurately capture shock wave and detonation propagation.

The computational domain is $0 \leq x \leq L$, where L is the chamber length. The initial distributions for temperature and mass fraction of all species are obtained from CHEMKIN PREMIX results such that the hot burned gas is on the left with $0 \leq x \leq 0.5$ mm and the unburned stoichiometric H_2 /air mixture at specified initial temperature of T_0 is on the right with $0.5 \text{ mm} \leq x \leq L$. Initially the flow is static ($u=0$) everywhere. The initial pressure of P_0 is uniformly distributed. Zero flow speed and zero gradients of temperature and mass fractions are enforced at the left ($x=0$) and right ($x=L$) boundaries. The premixed flame is initialized by the hot burned gas on the left and it propagates toward the end-gas on the right, which is continuously compressed. In order to track of the evolution of states of different material particles during autoignition, the flow particle tracking method (e.g., [31]) is adopted here.

3 Different autoignition cases

We conduct 1D simulations for different chamber lengths ($L=1, 2,$ and 4 cm) under a wide range of initial pressure ($P_0=2.5\sim 20$ atm) and temperature ($T_0=700\sim 1100$ K). Three typical autoignition cases listed in table 1 are observed for stoichiometric H_2 /air. The detailed results of these three cases are discussed below.

For case I with relative low initial temperature and pressure, end-gas autoignition does not happen. Fig. 1 shows that the temperature and pressure of end-gas continuously increase during flame propagation (the time sequence is indicated for different lines in the figure caption). However, there is no autoignition in end-gas since the ignition delay time is longer than the time that the end-gas close to $x=L$ is consumed by the propagating flame front (i.e., the value of the Livengood-Wu integral is less

than unity). It is noticed that the pressure is nearly uniformly distributed. This is because the pressure wave propagates at the speed of sound, which is much larger than the propagation speed of flame front. It is found that, when there is no end-gas autoignition, the pressure gradually increases to the adiabatic value of $P_e=29$ atm and the amplitude of pressure oscillation is within 2.5 atm.

Table 1 Three typical cases considered for stoichiometric hydrogen/air in a 1D closed chamber.

| Case | Chamber length | Initial pressure and temperature | Description |
|------|----------------|----------------------------------|-----------------------------|
| I | $L=2.0$ cm | $P_0=10$ atm, $T_0=900$ K | No autoignition |
| II | $L=2.0$ cm | $P_0=10$ atm, $T_0=1000$ K | Autoignition, no detonation |
| III | $L=1.0$ cm | $P_0=20$ atm, $T_0=1000$ K | Autoignition and detonation |

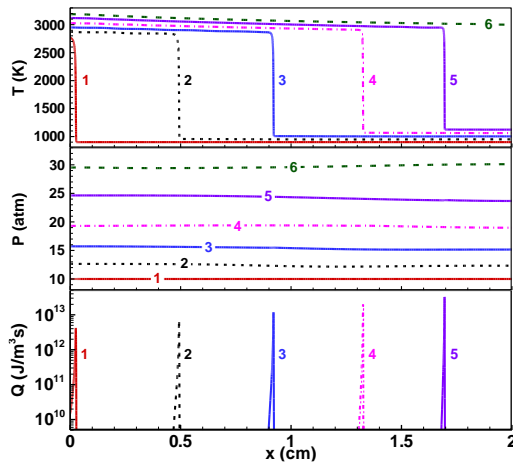


Fig. 1 Temporal evolution of temperature, pressure, and heat release rate distributions for case I ($L=2.0$ cm, $P_0=10$ atm, $T_0=900$ K). The time sequence is 1: 0 μ s, 2: 120.36 μ s, 3: 240.97 μ s, 4: 361.44 μ s, 5: 481.85 μ s, and 6: 602.36 μ s.

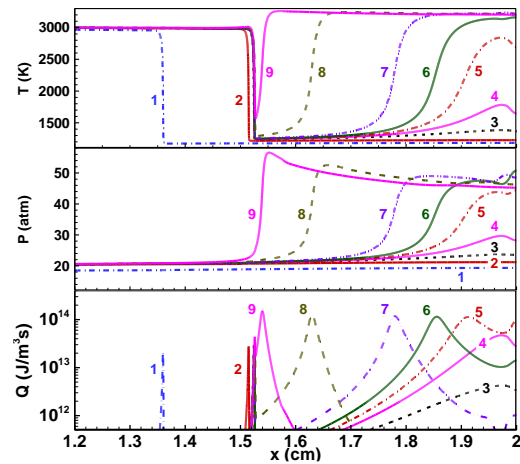


Fig. 2 Temporal evolution of temperature, pressure, and heat release rate distributions for case II ($L=2.0$ cm, $P_0=10$ atm, $T_0=1000$ K). The time sequence from line 1 to 9 is 282.81 , 320.83 , 323.68 , 323.83 , 323.91 , 323.99 , 324.15 , 324.62 , and 325.02 μ s.

When the initial temperature is increased from $T_0=900$ K to $T_0=1000$ K (case II), the ignition delay time is reduced and end-gas autoignition occurs. Fig. 2 shows that autoignition starts around $t_3=323.68$ μ s (line #3), when the temperature and pressure of end-gas are above 1200 K and 20 atm, respectively. The autoignition front (indicated by the heat release rate profile) is shown to propagate from the right boundary (i.e., $x=2$ cm) to the propagating flame front at around $x=1.52$ cm. After the autoignition front meets the flame front (see line #9 in Fig. 2), the mixture is consumed. It is noticed that the time difference between lines #9 and #3 is 1.34 μ s. Therefore, the average propagation speed of the autoignition front is around 3500 m/s, which is much higher than the speed of detonation, sound, and propagating flame front. Fig. 2 indicates that the local pressure increases due to the rapid heat release from autoignition. Since the reaction wave (autoignition front) is much faster than the acoustic wave, there is no coupling between them and the local maximum pressure is much less than that in a detonation shown below.

P-v diagrams for particles at different initial positions are plotted in Fig. 3 (a). Particles initially at $X_0=0.2$ and 1.0 cm pass through the flame before end-gas auto-ignition occurs. Therefore, they are adiabatically compressed before and after the transient heat release at nearly constant pressure. However, the particle initially at $X_0=1.9$ cm experiences first adiabatic compression due to right-propagating flame front, then transient heat release at nearly constant volume, and finally expansion. It is the nearly constant volume heat release that causes the sudden pressure rise observed in Fig. 2. The pressure rise generates pressure wave (much stronger than case I without autoignition) propagating back-and-forth in the closed chamber. Consequently, as shown in Fig. 3 (b), strong pressure oscillation occurs, which is

similar to the conventional knock observed by Wang et al. [3]. Therefore, end-gas autoignition can generate strong pressure waves which induce engine knock.

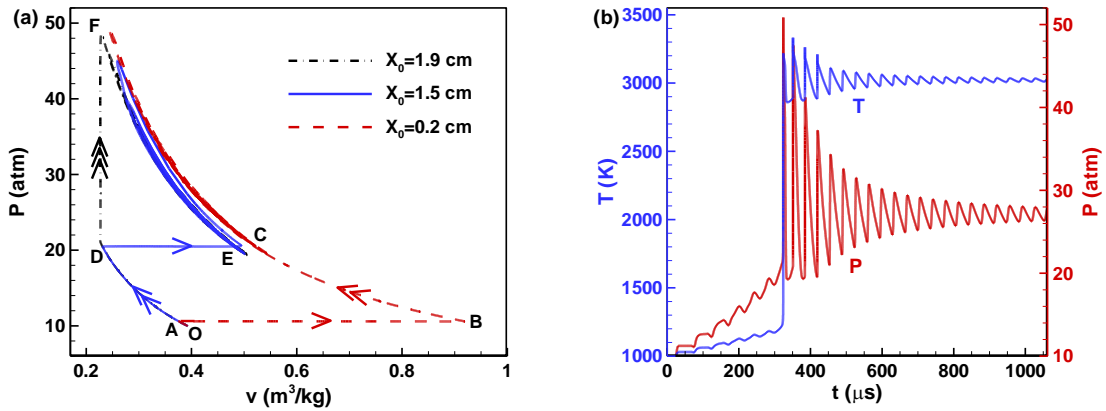


Fig. 3 (a) P-v diagrams for particles at different initial positions of $X_0=0.2, 1.5, 1.9$ cm (single arrow denotes constant-pressure combustion process; double arrow denotes compression process; and triple arrow denotes nearly-constant-volume ignition process); (b) Temporal evolution of temperature and pressure history at the right boundary (case II).

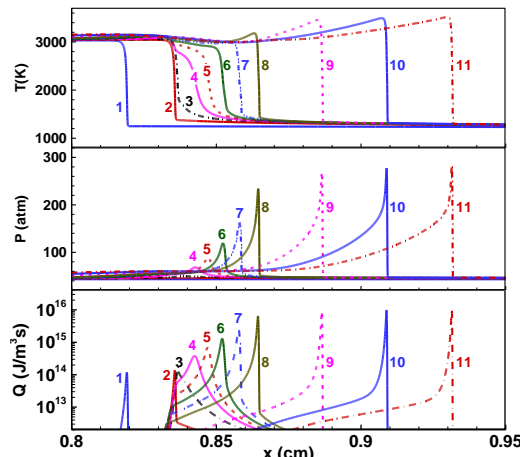


Fig. 4 Temporal evolution of temperature, pressure, and heat release rate distributions for case III ($L=1.0$ cm, $P_0=20$ atm, $T_0=1000$ K). The time sequence from line 1 to line 11 is 211.73, 216.44, 216.71, 216.78, 216.82, 216.86, 216.90, 216.94, 217.05, 217.17, and 217.28 μ s.

When the ignition delay time is further reduced by increasing the pressure to 20 atm (Case III), we observe end-gas autoignition and detonation as shown in Fig. 4. In our research, the main condition for detonation development is that the end-gas should be reactive enough so that it is on the threshold of autoignition. At $t=216.71$ μ s (line #3 in Fig. 4), the pressure is nearly uniformly distributed in the whole domain while there is obvious temperature gradient in the range of $0.836 \leq x \leq 0.846$ cm, which is in the upstream of the preheat zone. Such temperature gradient is caused by heat release from local autoignition and it can induce detonation development according to the theory of Zel'dovich [7, 10] on detonation generated by reactivity gradient. Autoignition first occurs around $x=0.836$ cm and the local heat release generates pressure pulse/wave propagating to the right, where the H_2 /air premixture is on the threshold of autoignition. The pressure wave initiates autoignition of this premixture, the heat release of which further strengthens the pressure wave. At the beginning (line #4 in Fig. 4), the pressure wave propagates much faster than the reaction/autoignition front. Then, the unburned end-gas immediately behind the pressure wave has higher reactivity after being compressed, which results in abrupt acceleration in the propagation speed (lines #4-8). Eventually, the enhanced coherent interaction between pressure wave and local chemical reaction leads to the formation of a self-sustaining detonation (lines #9 in Fig. 4).

The detonation development process can be further demonstrated by the P-v diagrams in Fig. 5 (a). Line #1 and line #2 correspond to particles pass through the flame front before autoignition happens. The particle corresponding to line #3 is located near the position where detonation development starts. It is observed that both P and v can increase along line #3. This is due to the interaction between heat release and expansion after pressure wave. The particles corresponding to line #4 and line #5 experience the transition to detonation. The particle corresponding to line #6 is shown to experience shock compression (from B to D) and then heat release (from D to E). Points D, E, and B is on a straight line (Rayleigh line). Therefore, the detonation is developed. The pressure history at the right boundary is shown in Fig. 5(b). It is observed extremely high pressure occurs when the detonation is reflected at the right boundary. Therefore, detonation development during end-gas autoignition can cause large amplitude pressure oscillation inside the closed chamber, which is similar to the super-knock observed by Wang et al. [3].

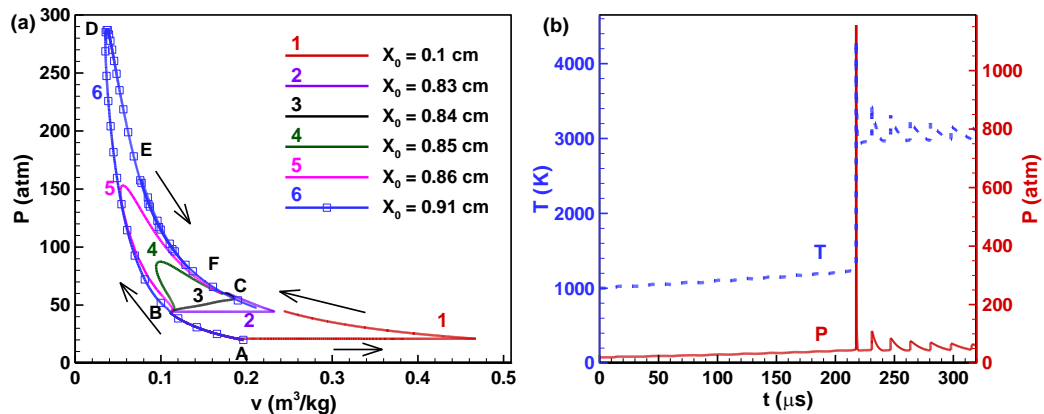


Fig. 5 (a) P-v diagrams for particles at different initial positions of $X_0=0.1, 0.83, 0.84, 0.85, 0.86, 0.91$ cm; (b) Temporal evolution of temperature and pressure history at the right boundary (case III).

4 Conclusions

Flame propagation and autoignition modes for stoichiometric H_2 /air in a 1D chamber is studied by numerical simulation considering detailed chemistry and transport. Depending on the initial temperature and pressure, three typical reaction modes for end-gas are observed: no autoignition, autoignition without detonation, and autoignition with detonation. The amplitude of pressure oscillation is small when there is no end-gas autoignition. However, when end-gas autoignition occurs, high amplitude of pressure oscillation is observed and knock occurs. Moreover, it is found that detonation development during end-gas autoignition can cause extremely high amplitude pressure oscillation inside the closed chamber. According to the analysis on pressure wave and reaction interaction, high reactivity, enough sensitivity of heat release to compression, and enough time for transition are crucial for detonation development during end-gas autoignition.

Acknowledgements

This work was supported by National Natural Science Foundation of China (Nos. 51322602 and 51136005) and State Key Laboratory of Engines at Tianjin University (No. K2014-01).

References

- [1] Wang Z et al. (2010). Combustion visualization and experimental study on spark induced compression ignition (SICI) in gasoline HCCI engines. *Energ Convers Manage.* 51: 908-917.
- [2] Kalghatgi GT, Bradley D. (2012). Pre-ignition and 'super-knock' in turbo-charged spark-ignition engines. *INT J ENGINE RES.* 13: 399-414.

- [3] Wang Z et al. (2015). Relationship between super-knock and pre-ignition. *INT J ENGINE RES.* 16: 166-180.
- [4] Heywood JB, (1988). *Internal Combustion Engines Fundamentals*. McGraw Hill. New York.
- [5] Bradley D et al. (1996). Heat release rates due to autoignition, and their relationship to knock intensity in spark ignition engines. *Proc. Combust. Inst.* 26: 2653-2660.
- [6] Pan J et al. (2014). Interaction of Flame Propagation and Pressure Waves During Knocking Combustion in Spark-Ignition Engines. *Combust Sci Technol.* 186: 192-209.
- [7] Zeldovich Y. (1980). Regime classification of an exothermic reaction with nonuniform initial conditions. *Combust Flame.* 39: 211-214.
- [8] Lee JHS. (2008). *The Detonation Phenomenon*. Cambridge University Press. Cambridge.
- [9] Livengood JC, Wu PC. (1955). Correlation of autoignition phenomena in internal combustion engines and rapid compression machines. *Proc. Combust. Inst.* 5: 347-356.
- [10] Zeldovich YB et al. (1970). On the development of detonation in non-uniformly preheated gas. *Acta Astronaut.* 15: 313-321.
- [11] Bradley D, Kalghatgi GT. (2009). Influence of autoignition delay time characteristics of different fuels on pressure waves and knock in reciprocating engines. *Combust Flame.* 156: 2307-2318.
- [12] Bradley D. (2012). Autoignitions and detonations in engines and ducts. *Philosophical Transactions of the Royal Society A: Mathematical, Physical and Engineering Sciences.* 370: 689-714.
- [13] Gu XJ et al. (2003). Modes of reaction front propagation from hot spots. *Combust Flame.* 133: 63-74.
- [14] Kawahara N et al. (2007). Auto-ignited kernels during knocking combustion in a spark-ignition engine. *Proc. Combust. Inst.* 31: 2999-3006.
- [15] Pöschl M, Sattelmayer T. (2008). Influence of temperature inhomogeneities on knocking combustion. *Combust Flame.* 153: 562-573.
- [16] Nagano Y et al., (2012). One-dimensional Flame Propagation and Auto-ignition of End Gas in Constant Volume Vessel. *The Eighth International Conference on Modeling and Diagnostics for Advanced Engine Systems (COMODIA 2012)*. Fukuoka, Japan.
- [17] Qi Y et al. (2013). Flame Propagation and End-gas Autoignition of Hydrogen/air Mixture in Closed Pipe. *Chinese Society of Engineering Thermophysics Combustion Session (Chinese Journal)*.
- [18] Reyes M et al. (2012). A method to determine ignition delay times for Diesel surrogate fuels from combustion in a constant volume bomb: Inverse Livengood – Wu method. *Fuel.* 102: 289-298.
- [19] Pan J, Sheppard CGW. (1994). A theoretical and experimental study of the modes of end gas autoignition leading to knock in SI engines. *SAE.* 942060.
- [20] Liberman MA et al. (2004). Numerical modeling of the propagating flame and knock occurrence in spark-ignition engines. *Combust Sci Technol.* 177: 151-182.
- [21] Luong MB et al. (2013). Direct numerical simulations of the ignition of lean primary reference fuel/air mixtures with temperature inhomogeneities. *Combust Flame.* 160: 2038-2047.
- [22] Yu R, Bai X. (2013). Direct numerical simulation of lean hydrogen/air auto-ignition in a constant volume enclosure. *Combust Flame.* 160: 1706-1716.
- [23] Ju Y et al. (2011). Multi-timescale modeling of ignition and flame regimes of n-heptane-air mixtures near spark assisted homogeneous charge compression ignition conditions. *Proc. Combust. Inst.* 33: 1245-1251.
- [24] Martz JB et al., (2012). The propagation of a laminar reaction front during end-gas auto-ignition. pp. 2077-2086.
- [25] Wang Z et al. (2012). Pressure oscillation and chemical kinetics coupling during knock processes in gasoline engine combustion. *Energ Fuel.* 26: 7107-7119.
- [26] Kagan LS et al. (2012). A minimal model for end-gas autoignition. *Combust Theor Model.* 16: 1-12.
- [27] Kagan L, Sivashinsky G. (2013). Hydrodynamic aspects of end-gas autoignition. *Proc. Combust. Inst.* 34: 857-863.
- [28] Dai P et al. (2014). Numerical experiments on reaction front propagation in n-heptane/air mixture with temperature gradient. *Proc. Combust. Inst.* 35.
- [29] Chen Z. (2010). Effects of radiation and compression on propagating spherical flames of methane/air mixtures near the lean flammability limit. *Article. Combust Flame.* 157: 2267-2276.
- [30] Li J et al. (2004). An updated comprehensive kinetic model of hydrogen combustion. *Int J Chem Kinet.* 36: 566-575.
- [31] Zhou R, Wang J. (2012). Numerical investigation of flow particle paths and thermodynamic performance of continuously rotating detonation engines. *Combust Flame.* 159: 3632-3645.